Article

From Aromatic Motifs to Cluster-Assembled Materials: Silicon–Lithium Nanoclusters for Hydrogen Storage Applications

Williams García-Argote , Erika Medel , Diego Inostroza , Alejandro Vásquez-Espinal , José Solar-Encinas , Luis Leyva-Parra * , Lina Ruiz * , Osvaldo Yañez * , William Tiznado *

Posted Date: 17 April 2025

doi: 10.20944/preprints202504.1420.v1

Keywords: hydrogen storage materials; silicon-lithium clusters; density functional theory; molecular dynamics; adsorption energy

 doi:10.20944/preprints202504.1420.v1

Article

From Aromatic Motifs to Cluster-Assembled Materials: Silicon–Lithium Nanoclusters for Hydrogen Storage Applications

Williams García-Argote [1], Erika Medel [2], Diego Inostroza [3], Alejandro Vasquez-Espinal [4], José Solar-Encinas [5], Luis Leyva-Parra [6,*], Lina Ruiz [7,*], Osvaldo Yañez [8,*] and William Tiznado [1,*]

[1] Centro de Investigación para el Diseño de Materiales (CEDEM), Facultad de Ciencias Exactas, Departamento de Ciencias Químicas, Universidad Andrés Bello, Avenida República 275, Santiago 837014,Chile

[2] Departamento de Química, División de Ciencias Básicas e Ingeniería, Universidad Autónoma Metropolitana, Iztapalapa, CP 09340 CDMX, México

[3] Departamento de Física, Facultad de Ciencias, Universidad de Chile, Ñuñoa, Santiago 7800024, Chile

[4] Química y Farmacia, Facultad de Ciencias de la Salud, Universidad Arturo Prat, Casilla 121, Iquique 1100000, Chile

[5] Laboratory of Theoretical Chemistry, Faculty of Chemistry and Biology, University of Santiago de Chile (USACH), Santiago, Chile

[6] Centro de Investigación en Ingeniería de Materiales (CIIM), Facultad de Ingeniería y Arquitectura, Universidad Central de Chile (UCEN), Santa Isabel 1186, Santiago 8370146, Chile

[7] Institute of Biomedical Sciences, Faculty of Health Sciences, Universidad Autónoma de Chile, Santiago, Chile

[8] Centro de Modelación Ambiental y Dinámica de Sistemas (CEMADIS), Facultad de Ingeniería y Negocios, Universidad de Las Américas, Santiago 7500975, Chile

* Correspondence: luis.leyva@ucentral.cl (L.P.); lina.ruiz@uautonoma.cl (L.R.); oyanez@udla.cl (O.Y.); wtiznado@unab.cl (W.T.)

Abstract: Silicon–lithium clusters are promising candidates for hydrogen storage due to their lightweight composition, high gravimetric capacities, and favorable non-covalent binding characteristics. In this study, we employ density functional theory (DFT), global optimization (AUTOMATON and Kick-MEP), and Born–Oppenheimer molecular dynamics (BOMD) simulations to evaluate the structural stability and hydrogen storage performance of key Li–Si systems. Potential energy surface (PES) exploration reveals that the true global minima of Li_6Si_6 and $Li_{10}Si_{10}$ differ markedly from previously proposed aromatic analogs based on benzene and naphthalene motifs. Instead, these clusters adopt compact geometries composed of one or two Si_4 (T_d) units and a Si_2 dimer, all stabilized by surrounding Li atoms. Motivated by the recurrence of the Si_4–T_d motif—previously shown to exhibit three-dimensional σ-aromaticity—we explore oligomers of Li_4Si_4, confirming additive H_2 uptake across dimer, trimer, and tetramer assemblies. Within the series of Si–Li clusters evaluated the $Li_{12}Si_5$ sandwich complex, featuring a σ-aromatic Si_5 ring encapsulated by two Li_6 units, achieves the highest hydrogen capacity, adsorbing 34 H_2 molecules with a gravimetric density of 23.45 wt%. Its enhanced performance arises from the high density of accessible Li^+ adsorption sites and the electronic stabilization afforded by delocalized σ-bonding. BOMD simulations at 300 and 400 K confirm dynamic stability and reversible storage behavior, while analysis of the interaction regions confirms that hydrogen adsorption proceeds via weak, dispersion-driven physisorption. These findings clarify structure-property relationships in Si–Li clusters and provide a basis for designing modular, lightweight, and thermally stable hydrogen storage materials.

 doi:10.20944/preprints202504.1420.v1

Keywords: hydrogen storage materials; silicon-lithium clusters; density functional theory; molecular dynamics; adsorption energy

1. Introduction

Hydrogen is widely regarded as a promising energy carrier due to its high gravimetric energy density, environmental compatibility, and potential role in decarbonizing multiple sectors of the global energy system. However, its practical implementation is limited by the lack of storage technologies that simultaneously ensure safety, reversibility, and efficiency under ambient or near-ambient conditions. Conventional storage methods such as high-pressure compression and cryogenic liquefaction suffer from energy inefficiency, safety risks, and low volumetric densities. In contrast, material-based hydrogen storage—where hydrogen is stored via physisorption, chemisorption, or a combination of both—has emerged as a compelling alternative. For such systems to be practical, adsorption energies must typically fall within the range of −0.1 to −0.8 eV per H_2 molecule, striking a balance between sufficient binding strength and reversible release under operational conditions[1–3]. Theoretical studies have shown that nanostructured materials—including metal-organic frameworks, functionalized carbon materials, and transition-metal-decorated systems—can meet these criteria by fine-tuning their surface electronic structure, pore architecture, and active site polarity[4–6]. Within this landscape, atomically precise clusters offer several intrinsic advantages, including high surface-to-volume ratios, tunable reactivity, and well-defined sorption sites, positioning them as promising candidates for high-performance hydrogen storage applications.

Various silicon–lithium (Si–Li) clusters have been proposed for hydrogen storage, supported by computational predictions of high gravimetric capacities and adsorption energies compatible with reversible, non-dissociative adsorption[7–11]. Particular attention has focused on aromatic clusters combining enhanced stability with favorable interaction profiles. Si_5Li_6 (C_{2v}), studied by Jena et al. in 2006, was predicted to adsorb up to 14 H_2 molecules, though steric constraints limit effective uptake to around 10, with adsorption energies of 0.11–0.16 eV per H_2 range[7]. Shortly thereafter, in 2012, Pan, Merino, and Chattaraj reported $Si_5Li_7^+$ (D_{5h}) and Si_4Li_4 (T_d) as viable hydrogen hosts, capable of storing 10–12 H_2 molecules with gravimetric capacities of 15.25 wt% and 14.7 wt%, and adsorption energies in the 0.10–0.20 eV per H_2 range[9]. Guo and Wang, in 2020, investigated $SiLi_4^+$, composed of a central Si atom tetrahedrally coordinated by Li atoms, which adsorbs 12 H_2 molecules at 30.2 wt% and ~0.12 eV per H_2, with dynamic stability confirmed at 300 K via molecular dynamics simulations[10]. All these clusters—Si_4Li_4, Si_5Li_6, $Si_5Li_7^+$, and $SiLi_4^+$—were confirmed as global minima (GM) through systematic potential energy surface (PES) exploration, reinforcing the reliability of their predicted properties[10,12–14]. In contrast, larger clusters such as Si_6Li_6 (D_{2h}) and $Si_{10}Li_{10}$ (C_s), proposed by Jaiswal and Sahu in 2022[8], were constructed without global optimization. While they were predicted to adsorb 18 and 40 H_2 molecules, respectively, with gravimetric capacities of 14.7 wt% and 18.7%, and adsorption energies ranging from 0.059 to 0.141 eV per H_2, their thermodynamic relevance remains uncertain. Larger silicon-based assemblies have also been proposed, including Li-functionalized $Si_{20}H_{20}$ frameworks with lithium-containing organic groups (e.g., CN_2HLi, CONHLi), reported in 2015 to adsorb up to 60 H_2 molecules (12.5 wt%) [15], and $Li_{12}Si_{60}H_{60}$, a 2009 silicon analog of a decorated fullerene, predicted to bind 30 H_2 molecules (7.46 wt%)[11] . However, these extended systems have not undergone global optimization, leaving their stability and practical viability unverified.

Cluster-assembled materials (CAMs)[16], constructed from discrete, atomically defined units that retain their structural and electronic identity upon aggregation, provide a robust framework for the modular design of functional nanomaterials[17]. In the realm of Si–Li systems, our computational studies have shown that Li_4Si_4 (T_d) and Li_6Si_5 (C_{2v})—both global minima—are promising building blocks stabilized by distinct forms of aromaticity. Li_4Si_4 exhibits spherical σ-aromaticity, while Li_6Si_5 features both σ- and π-aromatic delocalization. These clusters assemble into stable oligomers such as Li_8Si_8, $Li_{10}Si_9$, and $Li_{12}Si_{10}$, which preserve their local bonding environments and remain dynamically

 doi:10.20944/preprints202504.1420.v1

stable even at elevated temperatures[12]. Notably, these systems' Si_4^{4-} and Si_5^{6-} motifs are also present in experimental Zintl phases such as $Li_{12}Si_7$, Li_8MgSi_6, and $Li_{21}Si_5$, supporting their chemical viability[18–21]. Among these assemblies, $(Li_4Si_4)_n$ oligomers are particularly attractive for hydrogen storage due to their high density of surface-accessible Li^+ centers, which offer multiple binding sites for physisorption.

This study examines a series of structurally diverse Si–Li clusters selected for their potential to enable hydrogen storage via polar Li^+ adsorption centers, favorable charge distribution, and electronically stable, modular architectures. Although distinct in topology, all analyzed systems share a common underlying motivation: they are either based on aromatic Si–Li motifs or serve as computational models of CAMs with accessible surfaces for physisorption. Firstly, we revisit the Si_6Li_6 and $Si_{10}Li_{10}$ clusters, previously proposed as high-capacity sorbents due to their resemblance to benzene and naphthalene, respectively[8]. While these structures suggest delocalized bonding frameworks, they were modeled without global optimization, and their thermodynamic viability remains unresolved. We, therefore, carry out a comprehensive exploration of their potential energy surfaces (PES) to locate the true global minima and reassess their hydrogen adsorption properties. In addition, we analyze the $Li_{12}Si_5$ (D_5h) cluster[13], recently reported by our group as a global minimum sandwich-type system, built from a Si_5^{10-} ring flanked by two Li_6^{5+} units[13]. This compact, highly polarizable structure features σ-aromatic delocalization and a high density of Li^+ sites favorable for hydrogen binding. Finally, we investigate $(Li_4Si_4)_n$ oligomers (n = 1–3), which model CAMs based on the Li_4Si_4 (T_d) global minimum and exhibit a large number of accessible Li^+ adsorption sites. Together, these systems span a range of structural motifs and degrees of modularity, allowing us to examine the interplay between PES stability, electronic structure, and hydrogen uptake capacity in Si–Li nanocluster design.

2. Computational Details

The potential energy surfaces (PES) of the Li_6Si_6, $Li_{10}Si_{10}$, and $(Li_4Si_4)n$ (n = 1–3) clusters were explored using the AUTOMATON program[22], which combines a probabilistic automata-based framework with genetic algorithms, for the $(Li_4Si_4)n$ oligomers, PES exploration was also carried out using the guided Kick-MEP method[23]; full methodological details are provided in the Supporting Information. Initial structure screening for all systems was performed for singlet and triplet multiplicities at the PBE0[24]/SDDALL[25] level. Low-energy isomers within 20.0 kcal·mol^{-1} of the putative global minimum were re-optimized at the PBE0-D3[26]/def2-TZVP[27] level. Harmonic vibrational frequency calculations confirmed that all reported minima are true stationary points. Final relative energies were obtained from single-point refinements at the DLPNO-CCSD(T)[28]/CBS[29] //PBE0-D3/def2-TZVP level, carried out using ORCA 5.0.3; only these values are considered in the energetic discussion. Geometry optimizations and frequency calculations were performed using Gaussian 16[30]. All computational details and representative low-energy structures are included in the Supporting Information (Sections S1–S3).

Hydrogen adsorption energetics were evaluated by computing adsorption energies (E_{ads}) for all nH_2–cluster complexes using the expression:

$$E_{ads} = \frac{[E(complex) - nE(H_2) - E(cluster)]}{nH_2} \quad (1)$$

Here, E(complex) is the total energy of the hydrogen–cluster complex, $nE(H_2)$ is the energy of n isolated H_2 molecules, and E(cluster) is the energy of the bare cluster. To improve accuracy, adsorption energies were corrected for basis set superposition error (BSSE)[31] arising from artificial stabilization due to basis function overlap in weakly bound systems. Boys and Bernardi's counterpoise (CP) correction method was employed to account for BSSE[32]. The CP-corrected interaction energy (E_{CP}) is given by:

$$E_{CP} = E_{Int} - E_{BSSE} \quad (2)$$

 doi:10.20944/preprints202504.1420.v1

Here, Eint is the uncorrected interaction energy, and EBSSE is the basis set superposition error correction. All cluster geometries and their hydrogenated analogues were optimized using Gaussian 16 at the M06[33]/6-311+G(d,p)[34] level, chosen for its proven accuracy in describing dispersion-driven interactions relevant to hydrogen storage[8]. Practical storage capacity was estimated through gravimetric density calculations at approximate saturation using the expression:

$$\mathrm{wt\%} = \frac{\mathrm{M(nH_2)}}{\mathrm{M(nH_2) + M(cluster)}} * 100 \qquad (3)$$

Here, $M(nH_2)$ is the total mass of the adsorbed hydrogen molecules, and M(cluster) is the molecular mass of the bare cluster.

Non-covalent interactions were analyzed using the Independent Gradient Model based on Hirshfeld partitioning (IGMH)[35]. This method improves upon the original IGM method by using Hirshfeld-derived atomic densities, offering a more physically grounded and higher-resolution depiction of weak interactions. Compared to conventional NCI plots, IGMH provides more detailed insights into dispersion-driven adsorption. All analyses were performed at the M06/6-311+G(d,p) level using Multiwfn[36], with visualizations rendered in VMD[37].

To evaluate the structural resilience and reversibility of hydrogen adsorption under thermal conditions, Born–Oppenheimer molecular dynamics (BOMD)[38] simulations were conducted at 300 K and 400 K, temperatures relevant to practical hydrogen storage. The ADMP method[39], a Lagrangian formulation using Gaussian basis sets, was employed as a computationally efficient alternative to conventional BOMD, offering comparable accuracy for trajectory prediction. Simulations were run for 10 ps to assess structural stability and the dynamic retention of adsorbed hydrogen over time.

3. Results and Discussions

3.1. Confirming Li-Si Lowest Energy Structures

Figure 1 shows the global minima and the previously proposed high-symmetry structures for the Li_6Si_6 and $Li_{10}Si_{10}$ clusters[8], as identified through comprehensive PES exploration. For Li_6Si_6 (panel a, left), the global minimum exhibits C_s symmetry ($^1A'$ *state*) and is composed of a Si_4 tetrahedral unit (T_d) and a Si_2 dimer, surrounded by asymmetrically distributed Li atoms. This compact three-dimensional configuration is significantly more stable—by 20.4 kcal·mol^{-1}—than the previously proposed D_{2h}-symmetric structure (panel a, right), which features a planar Si_6 ring and had been modeled as a benzene analog in earlier hydrogen storage studies. For $Li_{10}Si_{10}$ (panel b), the global minimum adopts C_1 symmetry ($^1A'$ *state*) and consists of two Si_4 tetrahedra and one Si–Si dimer, coordinated by a spatially dispersed set of lithium atoms. This low-symmetry arrangement lies 52.0 kcal·mol^{-1} below the C_s-symmetric isomer (panel b, right), previously proposed as a naphthalene-like candidate for molecular hydrogen adsorption. These results indicate that the earlier high-symmetry, π-aromatic-like structures do not correspond to thermodynamically favored forms. Instead, the emergence of Si_4-based building units in both global minima highlight the stabilizing role of such substructures in lithium–silicon chemistry and supports their relevance for the design of hydrogen storage clusters. Additional low-energy isomers within 20 kcal·mol^{-1} of the global minima are reported in Figure S1-S2 (Supporting Information), further illustrating the structural diversity of these systems.

 doi:10.20944/preprints202504.1420.v1

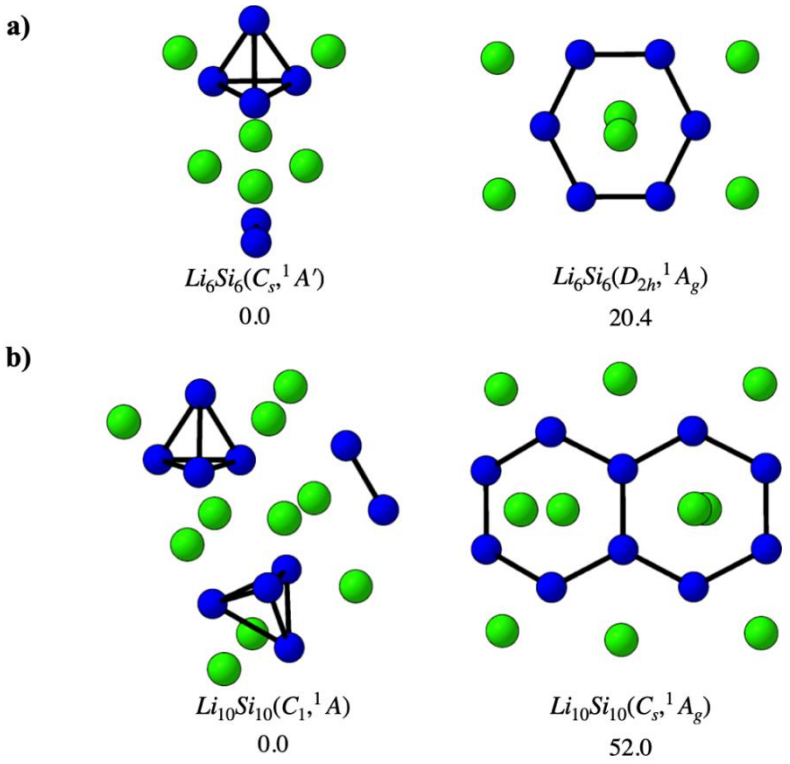

Figure 1. Global minima and previously proposed high-symmetry structures for (a) Li_6Si_6 and (b) $Li_{10}Si_{10}$ clusters. Relative energies are given in kcal·mol^{-1}, computed at the DLPNO-CCSD(T)/def2-TZVP//PBE0-D3/def2-TZVP level of theory.

In parallel with our identification of new global minima, we re-evaluated the potential energy surfaces of two previously proposed systems—$Li_{12}Si_5$ (D_5h, $^1A_1$) and the $(Li_4Si_4)_n$ oligomers (n = 2–3)—reported initially as global minima and selected here for their relevance to hydrogen storage. Our independent PES analysis confirms that these structures correspond to ground-state configurations. As shown in Figure 2, the Li_4Si_4 (T_d) monomer maintains its structural integrity upon oligomerization, with Li_8Si_8 and $Li_{12}Si_{12}$ preserving the local Si_4-based connectivity and Li^+ coordination. The $Li_{12}Si_5$ cluster was likewise verified to occupy the lowest point on the potential energy surface. These results substantiate the thermodynamic stability of the selected clusters and support their role as structurally persistent, modular building units for hydrogen-rich Si–Li assemblies.

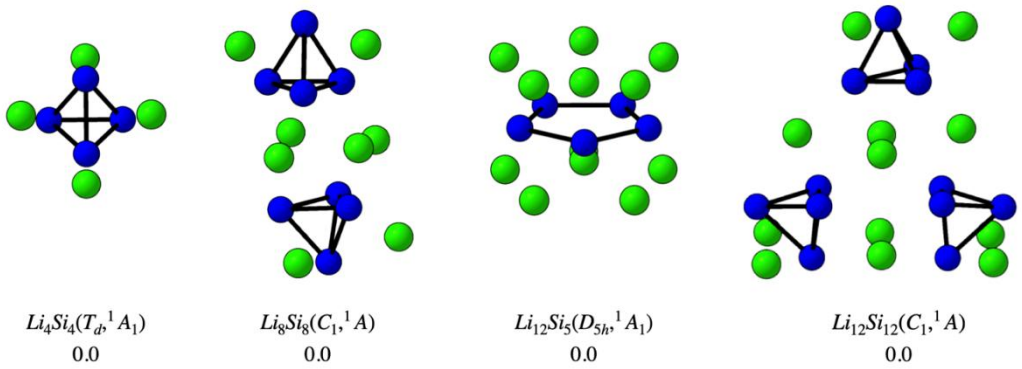

Figure 2. Optimized structures of global minima for the clusters Li_4Si_4, Li_8Si_8, $Li_{12}Si_5$, and $Li_{12}Si_{12}$, as confirmed in this work through potential energy surface (PES) exploration. All relative energies (in kcal·mol^{-1}) were computed at the PBE0-D3/def2-TZVP level of theory.

 doi:10.20944/preprints202504.1420.v1

3.2. Structural and Electronic Features of Bare and Hydrogen-Adsorbed Si–Li Clusters

Table 1 depicts the computed interatomic distances for the Si–Li clusters examined in this study and their corresponding hydrogen-adsorbed complexes. Si–Si bond lengths remain largely invariant upon H_2 adsorption, spanning 2.12–2.57 Å, reflecting the structural integrity of the silicon frameworks. Si–Li distances in the bare clusters range from approximately 2.40 to 2.76 Å and undergo modest elongation upon hydrogenation, particularly in larger assemblies such as Li_8Si_8 and $Li_{12}Si_5$, where maximum distances approach ~2.89 Å. Li–H separations offer insight into adsorption, with the shortest distances (2.08–2.30 Å) corresponding to favorable electrostatic interactions with exposed Li^+ centers. As hydrogen coverage increases, longer Li–H contacts—up to ~3.9 Å—are observed, indicating weaker physisorption at more peripheral or sterically hindered sites. This trend appears in both the global minimum (GM) structures identified through PES exploration and in the previously proposed high-symmetry local minima, Li_6Si_6* and $Li_{10}Si_{10}$*. While both structures support molecular hydrogen adsorption, the GM isomers generally present more spatially accessible and topologically diverse Li^+ coordination, which can enhance adsorption site availability. In all cases, H–H bond distances remain close to 0.75 Å, consistent with nondissociative molecular adsorption. These structural characteristics underscore the relevance of using thermodynamically validated GM structures for accurately predicting hydrogen storage performance in Si–Li clusters.

Table 1. Computed bond distances (in Å) for Si–Si, Si–Li, Li–H, and H–H interactions in bare Si–Li clusters and their hydrogen-adsorbed complexes, calculated at the M06/6-311+G(d,p) level of theory.

System	d_{Si-Si} (Å)	d_{Si-Li} (Å)	d_{Li-H} (Å)	d_{H-H}(Å)
H_2	-	-	-	0.74
Li_4Si_4	2.44	2.51	-	-
$4H_2$@Li_4Si_4	2.44	2.51-2.53	2.10	0.75
$8H_2$@Li_4Si_4	2.44	2.52-2.53	2.12	0.75
$12H_2$@Li_4Si_4	2.44	2.54-2.55	2.15-2.18	0.75
Li_6Si_6 (*)	2.31-2.36	2.40-2.76	-	-
$6H_2$@Li_6Si_6	2.31-2.35	2.41-2.76	2.09-2.16	0.75
$12H_2$@Li_6Si_6	2.31-2.34	2.42-2.73	2.08-3.58	0.75
$18H_2$@Li_6Si_6	2.31-2.34	2.42-2.75	2.09-3.47	0.75
Li_6Si_6	2.12-2.49	2.52-2.68	-	-
$6H_2$@Li_6Si_6	2.12-2.48	2.50-2.69	2.10-2.20	0.75
$12H_2$@Li_6Si_6	2.12-2.47	2.50-2.71	2.11-2.42	0.75
$18H_2$@Li_6Si_6	2.12-2.48	2.52-2.73	2.14-3.41	0.75
Li_8Si_8	2.35-2.54	2.44-2.89	-	-
$8H_2$@Li_8Si_8	2.36-2.52	2.47-2.73	2.09-2.26	0.75
$16H_2$@Li_8Si_8	2.36-2.51	2.50-2.72	2.12-2.29	0.75
$24H_2$@Li_8Si_8	2.36-2.51	2.49-2.71	2.14-3.46	0.75
$Li_{10}Si_{10}$ (*)	2.26-2.47	2.42-3.35	-	-
$10H_2$@$Li_{10}Si_{10}$	2.26-2.47	2.42-3.23	2.09-2.22	0.75
$20H_2$@$Li_{10}Si_{10}$	2.27-2.43	2.46-3.14	2.09-3.72	0.75
$30H_2$@$Li_{10}Si_{10}$	2.27-2.43	2.44-3.21	2.08-3.78	0.75
$Li_{10}Si_{10}$	2.13-2.53	2.47-2.85	-	-
$10H_2$@$Li_{10}Si_{10}$	2.13-2.52	2.46-2.94	2.09-2.25	0.75
$20H_2$@$Li_{10}Si_{10}$	2.13-2.51	2.49-2.85	2.12-3.55	0.75
$30H_2$@$Li_{10}Si_{10}$	2.13-2.50	2.51-2.85	2.13-3.90	0.75
$Li_{12}Si_5$	2.57	2.51-2.56	-	-
$12H_2$@ $Li_{12}Si_5$	2.46-2.57	2.49-2.59	1.93-2.17	0.75
$22H_2$@ $Li_{12}Si_5$	2.46-2.56	2.50-2.58	1.91-3.65	0.75
$24H_2$@ $Li_{12}Si_5$	2.44-2.56	2.50-2.60	2.13-3.81	0.75
$32H_2$@ $Li_{12}Si_5$	2.45-2.56	2.50-2.59	1.94-3.76	0.75

 doi:10.20944/preprints202504.1420.v1

34H_2@ $Li_{12}Si_5$	2.46-2.55	2.50-2.60	2.00-3.50	0.75
$Li_{12}Si_{12}$	2.39-2.52	2.47-2.71	-	-
12H_2@$Li_{12}Si_{12}$	2.38-2.48	2.47-2.72	2.10-2.30	0.75
24H_2@$Li_{12}Si_{12}$	2.37-2.52	2.47-2.67	2.11-3.20	0.75
36H_2@$Li_{12}Si_{12}$	2.36-2.52	2.49-2.67	2.13-3.47	0.75

* Local minimum obtained from the study of Jaiswal et al.

Table 2 compiles the HOMO–LUMO energy gaps (ΔE_{H-L}) of the studied lithium–silicon clusters, both in their bare and hydrogen-adsorbed configurations. These values offer insight into electronic stability and chemical hardness. Among the bare clusters, Li_4Si_4 exhibits the highest gap (3.1 eV), which increases to 3.4 eV upon adsorption of 8 H_2 molecules and remains relatively high (3.2 eV) for 12 H_2, confirming its closed-shell character and resilience to electronic perturbation. The global minimum structures of Li_6Si_6 and $Li_{10}Si_{10}$ show gaps of 2.8 and 2.6 eV, respectively, which are also maintained or even slightly enhanced upon hydrogenation, reaching 2.9 eV for both $12H_2$@Li_6Si_6 and $30H_2$@$Li_{10}Si_{10}$. In contrast, the previously proposed high-symmetry structures—Li_6Si_6* (D_{2h}) and $Li_{10}Si_{10}$* (C_s)—exhibit narrower gaps of 2.2 eV and 1.8 eV, respectively, with negligible changes upon hydrogen loading. These values match closely with those reported by Jaiswal et al., who found ΔE_{H-L} values of 2.33 eV for Li_6Si_6 and 1.81 eV for $Li_{10}Si_{10}$ using the B3LYP/6-31G(d,p) level of theory. Although method-dependent differences are expected, the trend is consistent: higher energy isomers on PES tend to display smaller HOMO–LUMO gaps and reduced electronic stability. Additional insights are observed in other systems. Li_8Si_8 displays an increase from 2.7 to 3.1 eV as H_2 adsorption progresses up to 16 molecules, followed by a decline to 2.1 eV at $24H_2$, suggesting a saturation threshold for electronic stabilization. $Li_{12}Si_{12}$ maintains gaps above 2.6 eV, while $Li_{12}Si_5$, the most compact and polarizable structure, shows the lowest gaps (1.3–1.7 eV), which increase modestly with hydrogen coverage.

Table 2. HOMO–LUMO energy gaps (ΔE_{H-L}, in eV) for the bare and hydrogen-adsorbed lithium–silicon clusters, calculated at the M06/6-311+G(d,p) level of theory.

System	E_{HOMO}	E_{LUMO}	ΔE_{H-L}
Li_4Si_4	−4.4	−1.3	3.1
4H_2@Li_4Si_4	−4.3	−1.0	3.3
8H_2@Li_4Si_4	−4.3	−0.9	3.4
12H_2@Li_4Si_4	−4.2	−1.0	3.2
Li_6Si_6 (*)	−3.6	−1.4	2.2
6H_2@Li_6Si_6	−3.6	−1.4	2.2
12H_2@Li_6Si_6	−3.5	−1.2	2.3
18H_2@Li_6Si_6	−3.6	−1.3	2.3
Li_6Si_6	−4.6	−1.8	2.8
6H_2@Li_6Si_6	−4.5	−1.6	2.9
12H_2@Li_6Si_6	−4.4	−1.5	2.9
18H_2@Li_6Si_6	−4.6	−1.8	2.8
Li_8Si_8	−4.4	−1.7	2.7
8H_2@Li_8Si_8	−4.4	−1.3	3.1
16H_2@Li_8Si_8	−4.3	−1.2	3.1
24H_2@Li_8Si_8	−3.4	−1.3	2.1
$Li_{10}Si_{10}$ (*)	−3.3	−1.5	1.8
10H_2@$Li_{10}Si_{10}$	−3.2	−1.4	1.8
20H_2@$Li_{10}Si_{10}$	−3.2	−1.4	1.8
30H_2@$Li_{10}Si_{10}$	−3.2	−1.4	1.8
$Li_{10}Si_{10}$	−4.3	−1.7	2.6
10H_2@$Li_{10}Si_{10}$	−4.2	−1.9	2.2
20H_2@$Li_{10}Si_{10}$	−4.1	−1.2	2.9

 doi:10.20944/preprints202504.1420.v1

30H_2@$Li_{10}Si_{10}$	−4.1	−1.2	2.9
$Li_{12}Si_5$	−3.0	−1.7	1.3
12H_2@ $Li_{12}Si_5$	−2.8	−1.2	1.6
22H_2@ $Li_{12}Si_5$	−2.7	−1.1	1.6
24H_2@ $Li_{12}Si_5$	−2.7	−1.1	1.6
32H_2@ $Li_{12}Si_5$	−2.8	−1.1	1.7
34H_2@ $Li_{12}Si_5$	−2.9	−1.2	1.7
$Li_{12}Si_{12}$	−4.0	−1.6	2.4
12H_2@$Li_{12}Si_{12}$	−3.9	−1.3	2.6
24H_2@$Li_{12}Si_{12}$	−3.9	−1.3	2,6
36H_2@$Li_{12}Si_{12}$	−3.9	−1.3	2.6

* Local minimum obtained from the study of Jaiswal et al.

3.3. Hydrogen Adsorption Energetics, Charge Redistribution, and Storage Capacity

The hydrogen adsorption properties of the investigated lithium–silicon clusters were assessed through BSSE-corrected adsorption energies (E_{ads}), partial charges on Li centers, and gravimetric hydrogen capacities (wt%), as summarized in Table 3. In all systems, Li atoms initially exhibit partial charges between +0.75 and +0.89, consistent with their role as electropositive adsorption sites. Upon hydrogen adsorption, these charges decrease progressively—reaching as low as +0.30 in $Li_{12}Si_5$—reflecting charge redistribution driven by weak donor-acceptor interactions. The BSSE-corrected Eads values lie within the optimal range for reversible hydrogen storage (−0.11 to −0.16 eV per H_2), with slightly stronger binding at low coverage. The difference from uncorrected values (~0.01–0.02 eV) confirms the weakly bound nature of the interactions and the importance of applying BSSE corrections for reliable energetic estimates. All PES-validated GM structures—Li_4Si_4, Li_6Si_6, Li_8Si_8, and $Li_{10}Si_{10}$—reach 14.72 wt% through adsorbing 12, 18, 24, and 30 H_2 molecules, respectively. These values align with the upper limit of approximately three H_2 molecules per Li^+, as Pan, Merino, and Chattaraj proposed[9]. Li_4Si_4, a symmetric and modular unit (T_d), and its oligomeric derivatives Li_8Si_8 and $Li_{12}Si_{12}$, maintain favorable adsorption behavior and extend capacity, with $Li_{12}Si_{12}$ reaching 14.72 wt% with 36 H_2. While the high-symmetry isomers of Li_6Si_6 (D_{2h}) and $Li_{10}Si_{10}$ (C_s) achieve comparable hydrogen uptake and adsorption energetics, they correspond to higher-energy local minima and show narrower Li charge distributions relative to the GMs. The $Li_{12}Si_5$ GM attains the highest capacity in the series (23.45 wt% with 34 H_2), enabled by its compact D_{5h} geometry, slightly stronger adsorption energies, and a broader Li charge range (+0.30 to +0.78), which reflects increased electrostatic heterogeneity across adsorption sites. For example, Figure 3 illustrates the stepwise hydrogen uptake over Li_8Si_8 and $Li_{12}Si_5$, showing progressive occupation of Li^+ centers with minimal structural deformation. These results demonstrate that the Si–Li GMs studied here combine thermodynamic stability, favorable charge redistribution, and optimal adsorption energetics to enable efficient and reversible hydrogen storage.

Table 3. Partial atomic charges on lithium centers (qLi), adsorption energies without (Eads) and with BSSE correction (Eads+BSSE) for hydrogen-adsorbed Li–Si clusters, computed at the M06/6-311+G(d,p) level of theory.

System	q(Li)	$E_{ads+BSSE}$ (eV)	E_{ads} (eV)	$wt\%$
Li_4Si_4	0.86	-	-	-
4H_2@Li_4Si_4	0.84	−0.12	−0.12	5.44
8H_2@Li_4Si_4	0.82	−0.12	−0.12	10.32
12H_2@Li_4Si_4	0.81	−0.11	−0.12	14.72
Li_6Si_6 (*)	0.83-0.84	-	-	-
6H_2@Li_6Si_6	0.81-0.85	-0.13	−0.14	5.44
12H_2@Li_6Si_6	0.81-0.82	-0.13	−0.13	10.30
18H_2@Li_6Si_6	0.82-0.83	-0.11	−0.11	14.72
Li_6Si_6	0.70-0.87	-	-	-

 doi:10.20944/preprints202504.1420.v1

$6H_2@Li_6Si_6$	0.70-0.84	−0.12	−0.13	5.44
$12H_2@Li_6Si_6$	0.72-0.82	−0.11	−0.12	10.30
$18H_2@Li_6Si_6$	0.72-0.81	−0.10	−0.11	14.72
Li_8Si_8	0.71-0.88	-	-	-
$8H_2@Li_8Si_8$	0.72-0.85	−0.12	−0.13	5.44
$16H_2@Li_8Si_8$	0.73-0.81	−0.11	−0.12	10.32
$24H_2@Li_8Si_8$	0.77-0.81	−0.10	−0.11	14.72
$Li_{10}Si_{10}$ (*)	0.74-0.87	-	-	-
$10H_2@Li_{10}Si_{10}$	0.75-0.85	−0.14	−0.14	5.44
$20H_2@Li_{10}Si_{10}$	0.75-0.83	−0.13	−0.13	10.32
$30H_2@Li_{10}Si_{10}$	0.76-0.83	−0.11	−0.12	14.72
$Li_{10}Si_{10}$	0.71-0.89	-	-	-
$10H_2@Li_{10}Si_{10}$	0.72-0.85	−0.12	−0.13	5.44
$20H_2@Li_{10}Si_{10}$	0.73-0.83	−0.11	−0.12	10.32
$30H_2@Li_{10}Si_{10}$	0.74-0.82	−0.10	−0.10	14.72
$Li_{12}Si_5$	0.30-0.78	-	-	-
$12H_2@Li_{12}Si_5$	0.63-0.84	−0.16	−0.17	9.76
$22H_2@Li_{12}Si_5$	0.60-0.82	−0.13	−0.14	16.54
$24H_2@Li_{12}Si_5$	0.59-0.81	−0.14	−0.14	17.78
$32H_2@Li_{12}Si_5$	0.60-0.82	−0.12	−0.13	22.38
$34H_2@Li_{12}Si_5$	0.63-0.82	−0.11	−0.12	23.45
$Li_{12}Si_{12}$	0.75-0.89			
$12H_2@Li_{12}Si_{12}$	0.76-0.85	−0.11	−0.12	5.44%
$24H_2@Li_{12}Si_{12}$	0.77-0.84	−0.11	−0.12	10.32%
$36H_2@Li_{12}Si_{12}$	0.78-0.83	−0.11	−0.11	14.72%

* Local minimum obtained from the study of Jaiswal et al.

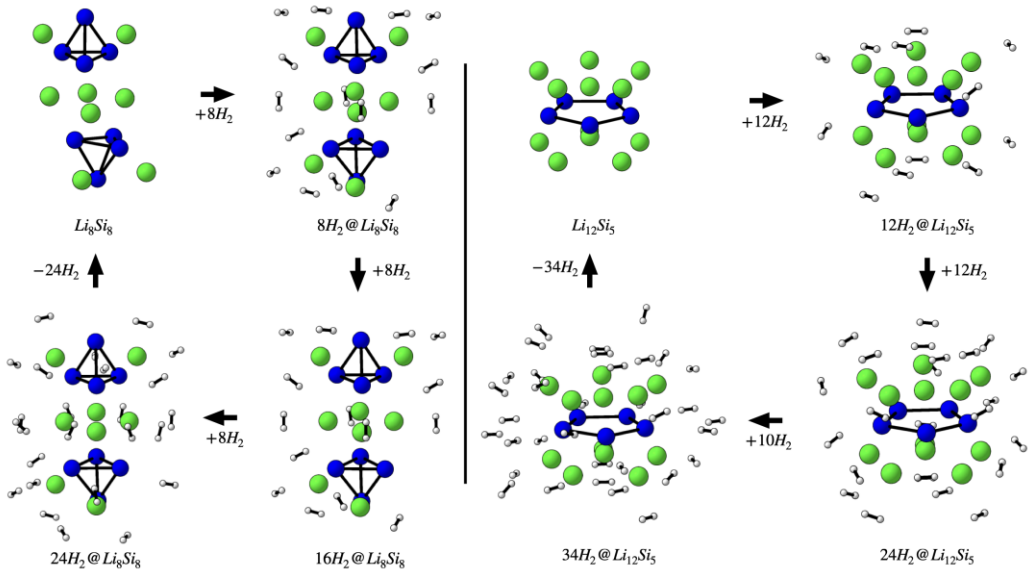

Figure 3. Sequential adsorption of H_2 molecules over Li_8Si_8 and $Li_{12}Si_5$ clusters.

3.3. Thermal Stability and Hydrogen Release Dynamics via BOMD Simulations

The reversibility and thermal resilience of hydrogen adsorption were assessed through Born–Oppenheimer molecular dynamics (BOMD) simulations on hydrogen-loaded Si–Li clusters: $12H_2@Li_4Si_4$, $18H_2@Li_6Si_6$, $24H_2@Li_8Si_8$, $30H_2@Li_{10}Si_{10}$, $34H_2@Li_{12}Si_5$, and $36H_2@Li_{12}Si_{12}$. Simulations were conducted for 10 ps at 300 K and 400 K to probe hydrogen release under operating conditions. As shown in Figures 4 and 5, desorption behavior depends strongly on cluster size. At 300 K, smaller

 doi:10.20944/preprints202504.1420.v1

clusters such as Li_4Si_4 and Li_6Si_6 release the majority of their adsorbed hydrogen within the first few picoseconds, with only 1–2 H_2 molecules retained by the end of the simulation. In contrast, larger systems like $Li_{12}Si_5$ and $Li_{12}Si_{12}$ retain 6 and 12 H_2 molecules, respectively, under identical conditions. This size-dependent stability becomes even more pronounced at 400 K, where small clusters undergo complete or near-complete desorption, while $Li_{12}Si_{12}$ maintains nearly one-third of its original hydrogen load. These observations confirm that increasing cluster size and coordination density enhances hydrogen retention under elevated thermal conditions.

A comparative analysis between PES-validated global minima (GM) and previously reported local minima (LM) structures for Li_6Si_6 and $Li_{10}Si_{10}$ (Figure 4) further underscores the role of structure optimization. While initial desorption rates are similar for GM and LM configurations, the GMs consistently retain more hydrogen at later times. For instance, at 400 K, $18H_2@Li_6Si_6$(GM) retains ~2 H_2 molecules, whereas the LM counterpart undergoes full desorption. Similarly, $30H_2@Li_{10}Si_{10}$(GM) retains ~4 H_2, while the LM form releases nearly all of its hydrogen content. These differences, though subtle in kinetics, reveal that GM structures offer more resilient binding sites capable of maintaining adsorbed hydrogen under thermal fluctuations. Altogether, the BOMD results support the conclusion that larger, PES-validated Si–Li clusters—particularly $Li_{10}Si_{10}$, $Li_{12}Si_5$, and $Li_{12}Si_{12}$—combine structural stability and dynamic retention, making them promising candidates for reversible hydrogen storage under realistic operating conditions.

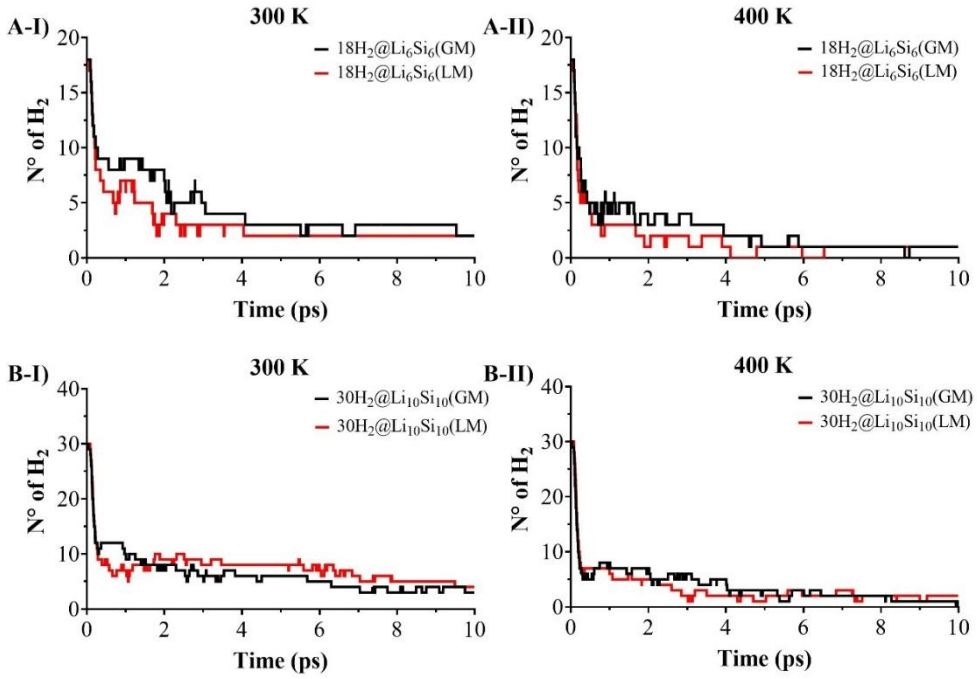

Figure 4. Hydrogen desorption dynamics of 18H2@Li6Si6 and 30H2@Li10Si10 clusters. Snapshots are shown after 10 ps of BOMD simulation at 300 K (A-I and B-I) and 400 K (A-II and B-II) for both global minimum (GM) and local minimum (LM, marked with *) structures. The LM configurations correspond to the geometries reported by Jaiswal et al.

 doi:10.20944/preprints202504.1420.v1

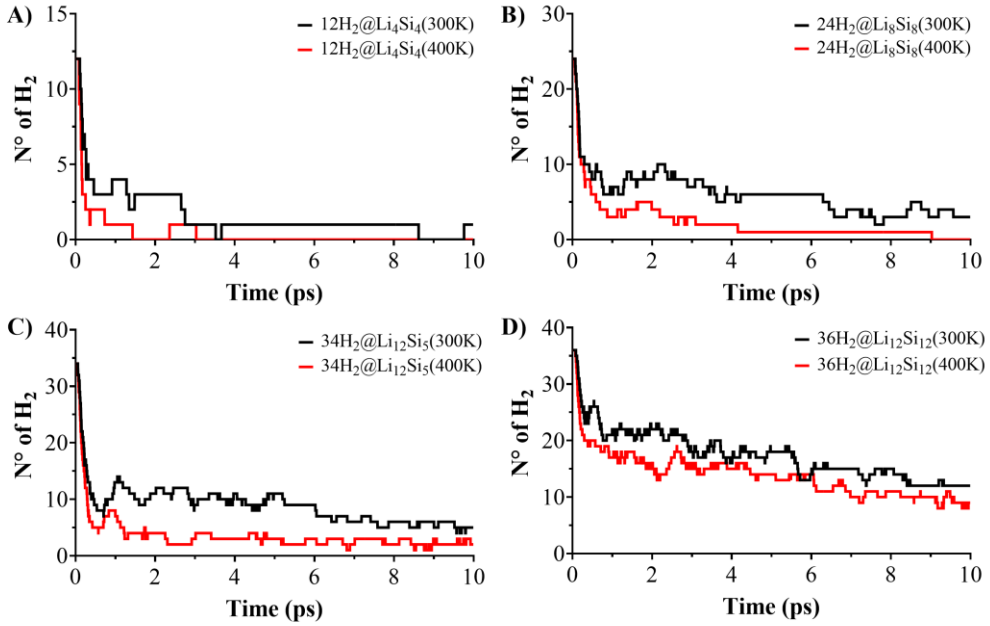

Figure 5. Hydrogen desorption profiles of selected H_2-loaded Li–Si clusters following 10 ps of BOMD simulation at 300 K and 400 K. Shown are final geometries for: (A) $12H_2@Li_4Si_4$, (C) $24H_2@Li_8Si_8$, (D) $34H_2@Li_{12}Si_5$, and (E) $36H_2@Li_{12}Si_{12}$. .

3.4. Visualization of Non-Covalent Interactions via IGMH Analysis

To gain visual insight into the nature of hydrogen adsorption in lithium–silicon clusters, we applied the Independent Gradient Model based on Hirshfeld partitioning (IGMH) to a series of representative hydrogenated systems (Figure 6). As a qualitative method, IGMH enables high-resolution visualization of non-covalent interactions by partitioning electron density based on the actual molecular environment, offering superior clarity compared to traditional NCI plots—especially for dispersion-dominated systems. In all cases, the interactions between H_2 molecules and Li^+ centers are characterized by green-colored isosurfaces located between the adsorbates and the cluster surface, confirming that physisorption is mediated primarily by weak van der Waals forces. No significant blue or red regions are observed, indicating the absence of strong electrostatic attractions or steric repulsion. The interaction fields are more extensive and homogeneously distributed in PES-validated structures such as $12H_2@Li_4Si_4$, $24H_2@Li_8Si_8$, and $34H_2@Li_{12}Si_5$, reflecting their favorable electrostatic landscapes and high hydrogen uptake. In contrast, the local minima geometries of $Li_6Si_6(D_{2h})$ and $Li_{10}Si_{10}(C_s)$ exhibit more fragmented interaction regions, correlating with reduced charge delocalization and lower retention in BOMD simulations. Overall, the IGMH results reinforce that dispersion-driven, non-dissociative physisorption governs hydrogen storage in these Si–Li clusters, complementing the energetic and dynamic analyses and validating their potential as reversible hydrogen carriers.

 doi:10.20944/preprints202504.1420.v1

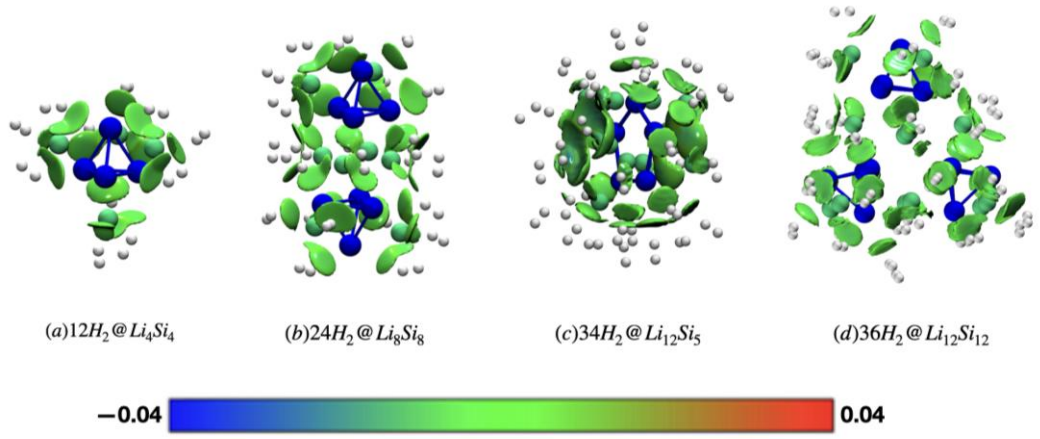

Figure 6. IGMH isosurfaces (δginter = 0.003 a.u.) for hydrogenated Li–Si clusters: (a) $12H_2@Li_4Si_4$, (b) $24H_2@Li_8Si_8$ (c) $34H_2@Li_{12}Si_5$, and (d) $36H_2@Li_{12}Si_{12}$. Calculations were performed at the M06/6-311+G(d,p) level of theory. Blue indicates attractive interactions, green represents weak or dispersive interactions, and red denotes repulsive regions. *Local minima reported by Jaiswal et al.

4. Conclusions

This study comprehensively investigates Si–Li clusters as hydrogen storage candidates, emphasizing the importance of accurate potential energy surface (PES) exploration. For the Li_6Si_6 and $Li_{10}Si_{10}$ systems, global optimization revealed that the true ground-state structures do not correspond to previously proposed benzene- and naphthalene-like motifs but rather consist of compact arrangements built from tetrahedral Si_4 (T_d) units and a Si_2 dimer, all stabilized by surrounding lithium atoms. Specifically, Li_6Si_6 features a single Si_4 unit and a Si_2 bridge, while $Li_{10}Si_{10}$ includes two Si_4 units linked via a Si–Si dimer. These findings highlight the necessity of PES validation in cluster-based materials design, ensuring that the predicted structures are electronically stable and experimentally feasible.

Guided by the recurrence of the Si_4–T_d motif, we evaluated oligomeric systems—dimers, trimers, and tetramers—of Li_4Si_4 as model cluster-assembled materials (CAMs). These oligomers preserve the local Si_4 environments and exhibit additive hydrogen storage behavior: each Li_4Si_4 unit binds 12 H_2 molecules (3 per Li^+), with total storage capacities increasing proportionally with the number of monomers. Additionally, we explored the aromatic $Li_{12}Si_5$ sandwich cluster, which incorporates a planar Si_5 ring stabilized by two Li_6 caps. This system achieves the highest gravimetric capacity in the series (23.45 wt%), attributable to its high density of accessible Li^+ sites. Collectively, our results establish clear structure–property relationships among Si–Li clusters and demonstrate the potential of PES-validated, modular architectures for designing thermally stable, high-capacity hydrogen storage materials.

Importantly, this work significantly advances the field of Li–Si clusters for hydrogen storage by delivering (i) a rigorous benchmark of global minimum structures for key systems previously proposed in the literature, (ii) new modular design principles based on Si_4–T_d building blocks, and (iii) the identification of high-performing sandwich-type and oligomeric clusters with verified thermodynamic and dynamic stability. These contributions provide a robust theoretical foundation for guiding future experimental development of silicon–lithium nanomaterials in next-generation hydrogen storage technologies.

Supplementary Materials: The following supporting information can be downloaded at the website of this paper posted on Preprints.org. Figure S1-S3: Putative global minimum and low-lying isomers of Li_6Si_6, $Li_{10}Si_{10}$ and $Li_{12}Si_{12}$,Figure S4: H_2 adsorption configurations,Table S1: T_1 diagnostics,Table S2: basis set superposition error,Table S3: Cartesian coordinates of the Li_4Si_4 , Li_8Si_8 ,Li_6Si_6, $Li_{10}Si_{10}$ and $Li_{12}Si_{12}$ optimized structures at the PBE0-D3/def2-TZVP level.

 doi:10.20944/preprints202504.1420.v1

Author Contributions: Conceptualization, W.T., L.L-P., W.G-A., and O.Y.; methodology, W.G-A., E.M., D.I., and O.Y.; software, W.G-A., D.I., E.M., and O.Y.; validation, W.G-A., L.L-P., and O.Y.; formal analysis, W.G-A., L.L-P., L.R., and D.I.; investigation, W.T., L.L-P., W.G-A., O.Y., E.M., D.I., J.S-E., L.R., and A.V-E.; resources, W.T., L.L-P., L.R., D.I., J.S-E., and A.V-E.; data curation, W.G-A., D.I., and O.Y.; writing—original draft preparation, W.G-A., L.R., L.L-P., O.Y. and W.T.; writing—review and editing, W.G-A., L.R., O.Y., W.T., L.L-P., E.M., D.I., J.S-E., and A.V-E.; visualization, W.G-A., L.R., and O.Y.; supervision, W.T., L.L-P., L.R., and O.Y.; project administration, W.T., L.L-P., L.R., and O.Y.; funding acquisition, W.T., L.L-P., L.R., and A.V-E. All authors have read and agreed to the published version of the manuscript.

Acknowledgments : This work was supported by the financial support of the National Agency for Research and Development (ANID) through FONDECYT project 1241066 (W. T.), FONDECYT project 1251871 (O. Y.) and FONDECYT project 1221019 (A. V.). Powered@NLHPC: This research was partially supported by the supercomputing infrastructure of the NLHPC (CCSS210001).

Conflicts of Interest: The authors declare no conflict of interest.

References

1. Jana, G.; Chattaraj, P. K., Exploring advanced nanostructures and functional materials for efficient hydrogen storage: a theoretical investigation on mechanisms, adsorption process, and future directions. *Front. Chem.* **2025,** 13, 1-13.
2. Jesse L. C. Rowsell, O. M. Y. P. D., Strategies for Hydrogen Storage in Metal–Organic Frameworks. *Angew. Chem.* **2005,** 44, (30), 4670-4679.
3. Zhou, W.; Yildirim, T., Nature and Tunability of Enhanced Hydrogen Binding in Metal–Organic Frameworks with Exposed Transition Metal Sites. *J. Phys. Chem. C.*. **2008,** 112, (22), 8132-8135.
4. Cychosz, K. A.; Matzger, A. J., Water Stability of Microporous Coordination Polymers and the Adsorption of Pharmaceuticals from Water. *Langmuir* **2010,** 26, (22), 17198-17202.
5. Liu, X.; Huang, D.; Lai, C.; Zeng, G.; Qin, L.; Wang, H.; Yi, H.; Li, B.; Liu, S.; Zhang, M.; Deng, R.; Fu, Y.; Li, L.; Xue, W.; Chen, S., Recent advances in covalent organic frameworks (COFs) as a smart sensing material. *Chem. Soc. Rev.* **2019,** 48, (20), 5266-5302.
6. Klontzas, E.; Mavrandonakis, A.; Tylianakis, E.; Froudakis, G. E., Improving Hydrogen Storage Capacity of MOF by Functionalization of the Organic Linker with Lithium Atoms. *Nano Lett.* **2008,** 8, (6), 1572-1576.
7. Jena, N. K.; Srinivasu, K.; Ghosh, S. K., Computational investigation of hydrogen adsorption in silicon-lithium binary clusters#. *J. Chem. Sci.* **2012,** 124, (1), 255-260.
8. Jaiswal, A.; Sahoo, R. K.; Ray, S. S.; Sahu, S., Alkali metals decorated silicon clusters (SiM, n = 6, 10; M = Li, Na) as potential hydrogen storage materials: A DFT study. *Int. J. Hydrogen Energy.* **2022,** 47, (3), 1775-1789.
9. Pan, S.; Merino, G.; Chattaraj, P. K., The hydrogen trapping potential of some Li-doped star-like clusters and super-alkali systems. *Phys. Chem. Chem. Phys.* **2012,** 14, (29), 10345-10350.
10. Guo, C.; Wang, C., Li center clusters MLi_4^+ (M = C, Si, Ge) for dihydrogen storage. *Int. J. Hydrogen Energy.* **2020,** 45, (46), 24968-24979.
11. Lan, J.; Cao, D.; Wang, W., $Li_{12}Si_{60}H_{60}$ Fullerene Composite: A Promising Hydrogen Storage Medium. *ACS Nano* **2009,** 3, (10), 3294-3300.
12. M.F.Manrique-de-la-Cuba; L.Leyva-Parra; D.Inostroza; B.Gomez; A.Vásquez-Espinal; J.Garza; O.Yañez; W.Tiznado, Li_8Si_8, $Li_{10}Si_9$, and $Li_{12}Si_{10}$: Assemblies of Lithium-Silicon Aromatic Units. *ChemPhysChem* **2021,** 22, (10), 906-910.
13. Inostroza, D.; Leyva-Parra, L.; Pino-Rios, R.; Solar-Encinas, J.; Vásquez-Espinal, A.; Pan, S.; Merino, G.; Yañez, O.; Tiznado, W., $Li_6E_5Li_6$: Tetrel Sandwich Complexes with 10-π-Electrons. *Angew. Chem.* **2024,** 136, (5), 1-7.
14. O.Yañez; V.Garcia; J.Garza; W.Orellana; A.Vásquez-Espinal; W.Tiznado, $(Li_6Si_5)_{2-5}$: The Smallest Cluster-Assembled Materials Based on Aromatic Si_5^{6-} Rings. *Chem. Eur. J.* **2018,** 25, (10), 2467-2471.
15. Song, B.; Zhang, C.; He, P., Si 20 H 20 cluster modified by small organic molecules and lithium atoms for high-capacity hydrogen storage. *Int. J. Hydrogen Energy.* **2015,** 40, (25), 8093-8105.
16. Khanna, S. N.; Jena, P., Assembling crystals from clusters. *Phys. Rev. Lett.* **1992,** 69, (11), 1664-1667.

 doi:10.20944/preprints202504.1420.v1

17. P.Jena; Q.Sun, Super Atomic Clusters: Design Rules and Potential for Building Blocks of Materials. *Chem. Rev.* **2018,** 118, (11), 5755–5870.
18. Nesper, R.; Curda, J.; Von Schnering, H. G., Li_8MgSi_6, a novel Zintl compound containing quasi-aromatic Si_5 rings. *J. Solid State Chem.* **1986,** 62, (2), 199-206.
19. Kuhn, A.; Sreeraj, P.; Pöttgen, R.; Wiemhöfer, H. D.; Wilkening, M.; Heitjans, P., Li NMR Spectroscopy on Crystalline $Li_{12}Si_7$: Experimental Evidence for the Aromaticity of the Planar Cyclopentadienyl-Analogous Si_5^{6-} Rings. *Angew. Chem.* **2011,** 50, (50), 12099-12102.
20. Köster, T. K. J.; Salager, E.; Morris, A. J.; Key, B.; Seznec, V.; Morcrette, M.; Pickard, C. J.; Grey, C. P., Resolving the Different Silicon Clusters in $Li_{12}Si_7$ by ^{29}Si and $^{6,7}Li$ Solid-State NMR Spectroscopy. *Angew. Chem.* **2011,** 50, (52), 12591-12594.
21. Hirsch, A.; Chen, Z.; Jiao, H., Spherical Aromaticity of Inorganic Cage Molecules. *Angew. Chem.* **2001,** 40, (15), 2834-2838.
22. Yañez, O.; Báez-Grez, R.; Inostroza, D.; Rabanal-León, W. A.; Pino-Rios, R.; Garza, J.; Tiznado, W., AUTOMATON: A Program That Combines a Probabilistic Cellular Automata and a Genetic Algorithm for Global Minimum Search of Clusters and Molecules. *Journal of Chemical Theory and Computation* **2019,** 15, (2), 1463-1475.
23. García-Argote, W.; Ruiz, L.; Inostroza, D.; Cardenas, C.; Yañez, O.; Tiznado, W., Introducing KICK-MEP: exploring potential energy surfaces in systems with significant non-covalent interactions. *J. Mol. Model.* **2024,** 30, (11), 369-382.
24. Adamo, C.; Barone, V., Toward reliable density functional methods without adjustable parameters: The PBE0 model. *J. Chem. Phys.* **1999,** 110, (13), 6158–6170.
25. P.Fuentealba; L.Von-Szentpaly; H.Preuss; H.Stoll, Pseudopotential calculations for alkaline-earth atoms. *J. Phys. B: Atom. Mol. Phys.* **1985,** 18, (7), 1287-1296.
26. S.Grimme; A.Jens; S.Ehrlich; H.Krieg, A consistent and accurate ab initio parametrization of density functional dispersion correction (DFT-D) for the 94 elements H-Pu. *J. Chem. Phys.* **2010,** 132, (15), 154104-154119.
27. F.Weigend; R.Ahlrichs, Balanced basis sets of split valence, triple zeta valence and quadruple zeta valence quality for H to Rn: Design and assessment of accuracy. *Phys. Chem. Chem. Phys.* **2005,** 7, (18), 3297-3305.
28. Purvis, G. D.; Bartlett, R. J., A full coupled-cluster singles and doubles model: The inclusion of disconnected triples. *J. Chem. Phys.* **1982,** 76, (4), 1910–1918.
29. Truhlar, D. G., Basis-set extrapolation. *Chem. Phys. Lett.* **1998,** 294, (1-3), 45-48.
30. M. J. Frisch, G. W. T., H. B. Schlegel, G. E. Scuseria, M. A. Robb, J. R. Cheeseman, G. Scalmani, V. Barone, G. A. Petersson, H. Nakatsuji, X. Li, M. Caricato, A. V. Marenich, J. Bloino, B. G. Janesko, R. Gomperts, B. Mennucci, H. P. Hratchian, J. V. Ortiz, A. F. Izmaylov, J. L. Sonnenberg, D. Williams-Young, F. Ding, F. Lipparini, F. Egidi, J. Goings, B. Peng, A. Petrone, T. Henderson, D. Ranasinghe, V. G. Zakrzewski, J. Gao, N. Rega, G. Zheng, W. Liang, M. Hada, M. Ehara, K. Toyota, R. Fukuda, J. Hasegawa, M. Ishida, T. Nakajima, Y. Honda, O. Kitao, H. Nakai, T. Vreven, K. Throssell, J. A. Montgomery, Jr., J. E. Peralta, F. Ogliaro, M. J.; Bearpark, J. J. H., E. N. Brothers, K. N. Kudin, V. N. Staroverov, T. A. Keith, R. Kobayashi, J. Normand, K. Raghavachari, A. P. Rendell, J. C. Burant, S. S. Iyengar, J. Tomasi, M. Cossi, J. M. Millam, M. Klene, C. Adamo, R. Cammi, J. W. Ochterski, R. L. Martin, K. Morokuma, O. Farkas, J. B. Foresman and D. J. Fox *Gaussian 16 Rev. C.01*, B.01; Gaussian Inc.: Wallingford, CT, 2016.
31. I. Mayer, P. R. S., Improved intermolecular SCF theory and the BSSE problem. *Int. J. Quantum Chem.* **1989,** 36, (3), 225-240.
32. Boys, S. F.; Bernardi, F., The calculation of small molecular interactions by the differences of separate total energies. Some procedures with reduced errors. *Mol. Phys.* **1970,** 19, (4), 553-566.
33. Zhao, Y.; Truhlar, D. G., The M06 suite of density functionals for main group thermochemistry, thermochemical kinetics, noncovalent interactions, excited states, and transition elements: two new functionals and systematic testing of four M06-class functionals and 12 other function. *Theor. Chem. Acc.* **2008,** 120, (1-3), 215-241.
34. Hehre, W. J., Ab initio molecular orbital theory. *Acc. Chem. Res.* **1976,** 9, (11), 399-406.

 doi:10.20944/preprints202504.1420.v1

35. Lu, T.; Chen, Q., Independent gradient model based on Hirshfeld partition: A new method for visual study of interactions in chemical systems. *J. Comput. Chem.* **2022,** 43, (8), 539-555.
36. T.Lu; F.Chen, Multiwfn: A multifunctional wavefunction analyzer. *J. Comput.Chem.* **2012,** 33, (5), 580-592.
37. Humphrey, W.; Dalke, A.; Schulten, K., VMD: Visual molecular dynamics. *J. Mol. Graph.* **1996,** 14, (1), 33-38.
38. J.M.Millam; V.Bakken; W.Chen; W.L.Hase; H.B.Schlegel, Ab initio classical trajectories on the Born–Oppenheimer surface: Hessian-based integrators using fifth-order polynomial and rational function fits. *J. Chem. Phys.* **1999,** 111, 3800–3805.
39. Iyengar, S. S.; Schlegel, H. B.; Voth, G. A., Atom-Centered Density Matrix Propagation (ADMP): Generalizations Using Bohmian Mechanics. *J. Phys. Chem. A.* **2003,** 107, (37), 7269-7277.